Spring 2019

Stress Corrosion Cracking of Stainless-Steel Reinforced Concrete

Nathan Frye
ncf9@zips.uakron.edu

Stress Corrosion Cracking of Stainless-Steel Reinforced Concrete

Nathan Frye

Department of Corrosion Engineering

Honors Research Project

Submitted to

The University of Akron Williams Honors College

Academic Supervisor: Dr. David M. Bastidas and Ulises Martin Diaz

April 26th, 2019

INDEX

Executive Summary

1. Problem:

There has been an increasing trend for the use of stainless steel rebar as a concrete structure reinforcing tool. Stainless steel is an iron alloy with a chromium content greater than 11%, allowing it to form its passive chromium oxide layer for corrosion protection. However this corrosion resistant film is jeopardized by the presence of chlorides, making it increasingly difficult to conduct proper life cycle costing analysis on structures near high chloride environments. This research is intended to analyze the relationship between the mechanical properties of the stainless steel rebar and the electrochemical environment change with increasing chloride content.

2. Results:

First examining the electrochemical results from the Linear Polarization Resistance (LPR) test, one of the key numerical values is corrosion rate. When observing the overall set of data, there is a trend of increasing and decreasing corrosion rate values from as low as 0.476 mpy (mils per year) to as high as 1.518 mpy and back down. This phenomena is thought to be the passivity breakdown and repassivation of this protective oxide film on the surface of the metal, leading to periodic corrosion rates. Fractographic studies of the failure also indicate the presence of corrosion product in the samples with Cl^- present, something that was not seen in the blank tests. This is thought to accelerate the failure by assisting the tensile machine in separating the metal. Lastly, when observing the mechanical properties from a stress/strain curve, we saw a ~7.7% decrease in ultimate tensile strength between the blank sample and that of the 8% Cl^- sample.

3. Conclusions:

Although limited by the results gathered in this report relative to the amount of work to still be done, there was success in these tests. The electrochemical tests showed signs of the passive film breakdown due to Cl^- ions and consequential accelerated corrosion rates. These corrosion rates then translated into the mechanical tensile test and yielded lesser ultimate tensile strength as well as yield strength. The remaining samples and tests will be conducted over the months to come with Ulises and Dr. Bastidas to complete this study and reach our goal.

4. Implications of Work:

This research conducted with Dr. Bastidas has been my first experience with true research and development. My Co-op experience did not ever reach this side of the industry and it was an area that I was not the most proficient in. After a year of assisting in sample preparation, equipment construction and result analysis I have gained life skills that will transfer to my full time position with Marathon Petroleum Corporation. Some tasks such as finding the proper chemical etchant took upwards of six tries to finally reach the desired result; teaching me perseverance. Another important skill gained from this research was from writing the report itself. Dr. Bastidas consistently stressed the importance a proper research document carries and its reflection on the author.

The overall outcome of this research project is to create a better and safer world. The stainless steel being tested is currently being used to create buildings and infrastructure for public use. The corrosion research we can provide to the industry will allow in more accurate life span calculations and potentially save lives in the future by preventing unexpected failures. With this information, more accurate cost benefit analysis calculations will be able to be made, diminishing maintenance

and repair cost, and perhaps persuading companies to choose stainless steel rebar as opposed to the more commonly used carbon steel. There is also an environmental impact to be considered. By improperly choosing materials with short failure times, it increases the need for new raw materials and construction. By building these structures to last for the long term, it is reduced the need for harvesting of the raw materials and construction of the final product.

5. Recommendations:

With respect to the importance of this topic, further research will need to be conducted. The end goal of creating a model or developing a relationship between such chloride solution concentration and effect on the life span of the stainless steel rebar is no easy task. Although this report only reflects the stainless steel AISI 316 results, further tests will be conducted on the remaining alloys. The mechanism of crack growth for stress corrosion cracking is a controversial topic and needs to be further tested in multiple scenarios to better understand it.

Honors Abstract Addendum

Stainless steel rebar is one of the most corrosion resistant reinforcing methods for concrete structures. Stainless steel is used for its chromium content and its ability to form a passive oxide corrosion resistant layer. The presence of chloride is one of the largest attackers of this passive film and able to penetrate concrete due to its porous characteristics. This study evaluates the mechanical performance of different stainless steels relative to their changing environments. It is expected that as chloride concentration values increase, mechanical properties will decrease. This will be tested by performing tensile tests on stainless steel rebar sample that is enclosed in a galvanic cell. Electrochemical tests such as Linear Polarization Resistance and Electrochemical Impedance Spectroscopy will also be performed during the tensile test to examine the relationship during this time. To this point, only results from the AISI 316 SS have been completed, showing that the 8% chloride concentration solution performed nearly 7.7% worse than the blank sample during mechanical tensile tests. An accurate relationship between mechanical properties and environment allows for more accurate life cycle costing analysis of materials during construction.

1. Introduction

In the design stages of a new bridge, building, or tower, material selection is of upmost importance. These concrete structures will need to be reinforced with additional support from a wide variety of options such as epoxy coated rebar, galvanized rebar, and polymer reinforced rebar. However, in certain applications the lifecycle cost benefit analysis leads to no other choice than the use of stainless steel rebar. Stainless steel is an alloy of iron with a minimum concentration of approximately 11% chromium [5]. Chromium is added to provide corrosion protection by preferentially oxidizing over iron to form Cr_2O_3. This oxide layer is a thin film and acts as a protective barrier and is commonly referred to as a passive layer. Stainless steel rebar is used for its ability to form this protective passive film, its mechanical properties, and low magnetic permeability [1]. In areas with an aggressive environment and high chloride concentration such as the ocean, the passivated film from the stainless steel is degraded. For this reason, the experiment will focus around developing a relationship between chloride concentration and overall failure limit of the stainless steel rebar. Effectively linking the electrochemical environment to the mechanical properties of the metal. This will therefore allow for more accurate lifespan calculations as well as material selection cost analysis.

The corrosion of reinforcing rebar is one of the main causes of mechanical failure in these structures. The mechanism of corrosion that will be evaluated in this report is stress corrosion cracking (SCC). SCC is defined as the growth of cracks due to the simultaneous action of tensile stress while combined with a corrosive environment such as chloride ions, water, oxygen, and pH [2]. This tensile stress can be introduced to the metal in a few ways; heat treating, welding, or direct mechanical tension. Only a very specific combination of alloys, tensile stress, and environment can allow for SCC to occur.

Stainless steels are commonly divided into five groups; austenitic, ferritic, martensitic, duplex, and precipitation hardening [5]. In this experiment austenitic stainless steel AISI 316 will be analyzed. Austenitic stainless steels are the most commonly used type of stainless steel for industrial and consumer applications. Austenites face-centered cubic (FCC) structure allows it to hold high proportion of carbon in solution, leading to its high weldability and formality. [7] Duplex stainless steel on the other hand gets its name from its dual composition microstructure of roughly 50% austenite and 50% ferrite [12]. As mentioned previously, austenite contains an FCC structure while ferrites structure is body-centered cubic (BCC). Duplex stainless steels contain 22-25% chromium and are known for their higher yield strength and stress corrosion cracking resistance to chloride. [6]. Lean-duplex stainless steel can be classified as a less alloyed version of duplex stainless steel In this instance, there is less chromium content but more importantly less nickel in the composition. Nickel is an important factor when alloying these stainless steels. Its primary function is to promote the austenite phase, so that predominantly austenitic and austenitic-ferrite alloys can be produced. By adding enough Ni the austenite range can be stabilized at room temperature and below. [8] When alloying any metal, another important factor is cost. Nickel is one of the most expensive common metal alloying elements, ranging from $6 per pound to as high as $9 per pound in some exchanges [9]. Comparatively to other alloying elements such as manganese, copper, and aluminum at rates of $3.00, $2.94, and $0.84 respectively. [10] With such a cost impact on the product, lean alloyed stainless steels are offered as a cheaper alternative. In the industry, carbon steel rebar is referred to as “black bar” and is used for its cheap value/tensile strength ratio [11].

For the environment, an electrochemical cell was designed to fit around the rebar, allowing for the simulation of a concrete environment during testing. This container allows for the introduction of a saturated calomel reference electrode and graphite counter electrode in order to monitor the corrosion related properties during testing. A GAMRY potentiostat was then connected to these electrodes in order to run the electrochemical tests such as Linear Polarization Resistance and Electrochemical Impedance Spectroscopy.

The porous concrete environment will be simulated by using a saturated calcium hydroxide solution. According to the Institute for Research in Construction, calcium hydroxide has a significant role in determining the mechanical performance and volume stability of cementitious materials. [30] This environment will also allow visual inspection of the sample during tensile testing while also properly representing the concrete, rebar relationship.

This solution will then have a particular chloride concentration added in order to see how the fracture mechanics of the samples react to a change in environment. A “blank”, or control test was also run to introduce a control variable to the experiment. It is important to note that the control test was not exposed to air. Rather this test was also in a calcium hydroxide solution with no chloride present. These chloride concentrations were chosen in reference to the average chloride concentration of seawater. The vast majority of seawater is found in oceans with in average salinity of approximately 3.5% [13].

Lastly, the stress element will be introduced through a tensile testing machine. The rebar and electrochemical cell will be loaded into a static, lower arm, while the top is stretched upwards. Tensile tests are performed to test a materials mechanical properties; ensuring that proper specifications are met. Tensile tests are also used to predict the behavior of a material under forms of loading other than uniaxial tension [14].

To begin the tensile test, the rebar had to be prepared accordingly. The standard tensile specimen is composed of a shoulder and gauge section, with the gauge section being the area of interest [14]. The specimen will be secured in the machine at the shoulders. In this instance a tool was used to create a mechanical thread on the end of the rebar, to later be screwed into the specimen holder. Once threaded, the next step was to introduce a notch to the center of our sample, following the ISO 7539-11 standard [3]. When creating this notch, it was important to have consistent samples throughout each test. This will eliminate the possibility of an external factor acting on the tensile test results. Reinforcing rebar contains two longitudinal ribs and ascending inclined transverse ribs to bind it mechanically to the concrete [16]. Therefore the design specification used in these experiments calls for the notch was to be perpendicular to a longitudinal rib. The final step of sample preparation included coating the sample in a red lacquer paint. However, a 5 millimeter span above and below the notch was left uncoated. This was to ensure that all electrochemical testing will be focused on the notch and crack tip of the rebar.

During tensile testing, a fundamental relationship between stress and strain is used to describe the materials properties. Where true strain is defined by change in length divided by original length and true stress is defined by force per unit area. This stress-strain curve will allow us to measure a materials ductility, modulus of elasticity, and overall displacement. However, with the notch being introduced to our sample, the rebar no longer has a uniform circular cross section. For this reason, we will be using what is referred to as engineering stress/strain; an approximation of these values.

When performing the tensile test, the material specification sheet will be used to identify two key parameters; ultimate tensile strength (UTS) and yield strength. The yield point is the maximum load the sample can hold before entering plastic deformation. While the ultimate tensile

strength is the maximum load the sample can hold before experiencing necking and eventually failure. At the conclusion of our tensile test, the data was fit with parameters of 50, 75, and 100% yield strength, and later 80, 90, 100% of UTS. It was during these windows of loading that the electrochemical tests were being performed. This was done to monitor the electrochemical response of the transition of elastic to plastic deformation and allow us to observe any changes.

Through this stress corrosion cracking mechanism, failure is expected to occur in a two-phase system, corrosion initiation and corrosion propagation [4]. The corrosion initiation at the crack tip will generate corrosion product buildup, which in such a confined space can generate additional stresses and lead to accelerated corrosion propagation. This is the stress that will be affected by the concentration of the chloride; the faster and more aggressive the corrosion product builds up, the faster the failure will occur. For this reason, stress corrosion cracking is what is known as a delayed failure process; with slow initiation and rapid propagation [18].

There are multiple theorized models of stress corrosion cracking mechanisms for stainless steel alloys. There is no universal model that explains the mechanisms proposed for SCC due to the inconsistency of data, however most can be broken down into anodic or cathodic models. A popular theorized mechanism is the film rupture model where the crack tip grows by anodic dissolution when the film is ruptured [2]. This model takes into consideration the cyclic breakdown of the protective film, crack growth, and then repassivation of the metal. Results under this model would have varying corrosion rates depending on the status of the chromium oxide layer.

To analyze the fracture mechanics of the rebar, an optical light microscope will be used to take macroscopic images. The two main modes of failure in metals are ductile failure and brittle failure. Also known as cup-and-cone failure, ductile failure is a slow mode of cracking where the material pulls apart, generally leaving behind a shear lip. Brittle failure on the other hand is a rapid

failure with no plastic deformation and sudden separation in the form of transgranular fracture or intergranular fracture. In order to observe these precise details, a scanning electron microscope (SEM) will be used. The SEM machine has much better resolution and depth of field that can identify surface features of the fracture [19].

2. Experimental Methods

The experiments conducted during this research can be categorized into four groups. Group 1 testing methods consists of multiple tests that were ran simultaneously. The overall procedure being ran is the slow strain rate testing, or constant extension tensile testing while the subsequent electrochemical tests were being performed: Linear Polarization Resistance, Electrochemical Impedance Spectroscopy, and Open Circuit Potential runs. Group 2 is fractography, where analysis will be conducted on the failed rebar by optical light microscopes as was as scanning electron microscopes to better analyze the mechanism of failure. Group 3 consists of metallography, or the study of the microstructure of the metal. Lastly, Group 4 consists of the electrochemical test; Cyclic Potentiodynamic Polarization. Being a destructive testing method, this test was done on a different sample in a separate corrosion cell.

(1) Slow Strain Rate Testing

Also known as a constant extension rate test, the purpose of this step is to introduce a tensile stress to our sample. The process for performing this test uses an electromechanical tensile machine with threaded inserts. The rebar sample is first screwed into the base of the tensile machine before the electrochemical cell is inserted above and secured. The cell is then filled with the designated calcium hydroxide mixture. After the lid is placed on the cell, the counter electrode and reference electrode are inserted and connected to the GAMRY Potentiostat. Once the upper arm of the tensile machine is attached to the sample, the machine is then pre-loaded to 100 kilogram-force. Being a constant extension test, the tensile machine is then set to increase at a rate of $1X10^{-6}$ inches per second based off of ASTM-G129, “Standard Practice for Slow Strain Rate Testing to Evaluate the Susceptibility of Metallic Materials to Environmentally Assisted Cracking” [32]. **Figure 1**

below shows the complete set up of the tensile testing machine along with additional images in the appendix.

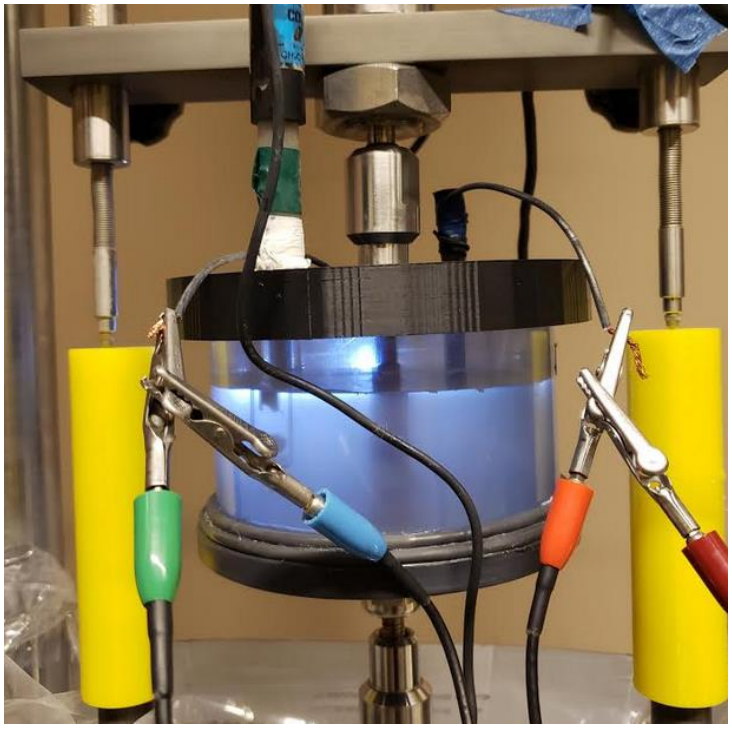

Figure 1 – Complete set up of electrochemical cell in tensile testing machine along with counter electrode (Red/Orange), working electrode (Blue/Green) and reference cell (White, not shown)

OCP Testing

The open circuit potential, (OCP) of a metal is the potential of the working electrode relative to the reference electrode when there is no current being applied. This value is important when attempting to understand the thermodynamic tendency of the metal. Metals with a more noble OCP are more thermodynamically stable than those with a lower OCP [20]. These values are taken to essentially measure the electrochemical potential of the solution and give a reference to values gained through other testing methods. For our tests, the length of each open circuit potential run lasted 3600 seconds, gathering information every 1 second.

Linear Polarization Resistance (LPR)

Linear polarization resistance (LPR) is a common non-destructive testing technique used to study the corrosion rate of a metal. For this test, the working electrode is polarized ±15 mV relative to its open circuit potential (OCP) [21]. As the sample is polarized, a current is introduced and the relationship between the two is monitored using basic Ohm's Law principles V=IR, producing a resistance value, Rp (polarization resistance). For such a small polarization deviation from the OCP, the expected response would be a linear relationship. The slope of this relationship, voltage divided by current, is defined as the polarization resistance, Rp. This polarization resistance (ohms) can be used to calculate the instantaneous corrosion rate of the cell through the use of the Stern-Geary equation shown below [22, 26]. (Where βa and βc are the anodic and cathodic Tafel slopes). **Figure 2** on the following page is in reference to test parameters used for LPR tests.

$$Rp\ (ohms) = \frac{\beta_A \beta_c}{2.3 * (i_{corr}) * (\beta_A + \beta_c)} \quad (1)$$

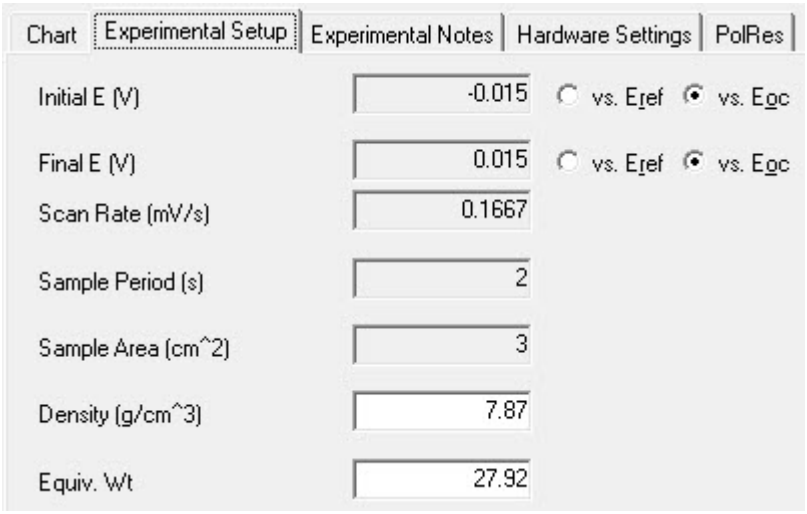

Figure 2 – Test parameters used for the Linear Polarization Resistance experiment used in the GAMRY Software.

Electrochemical Impedance Spectroscopy (EIS)

Electrochemical Impedance Spectroscopy is another common testing technique used to study corrosion behavior of stainless steel. Similarly to the linear polarization resistance technique, a small potential is applied to the sample, however in EIS testing this is an AC voltage. Some advantages of using EIS over other electrochemical techniques are its measurement over a wide frequency range, ability to make high precision measurements, and the ability to gather impedance data. This test essentially measures the electrochemical response to an AC voltage being applied at different frequencies [27]. This reaction is then interpreted by fitting the graph to an equivalent circuit model. These results can be plotted in terms of frequency and phase angle vs impedance modulus (Bode Plot) or in terms of imaginary vs. real components of impedance (Nyquist Plot). **Figure 3** on the following page is in reference to test parameters used for EIS tests and **Figure 4** shows the equivalent circuit model used for data fitting.

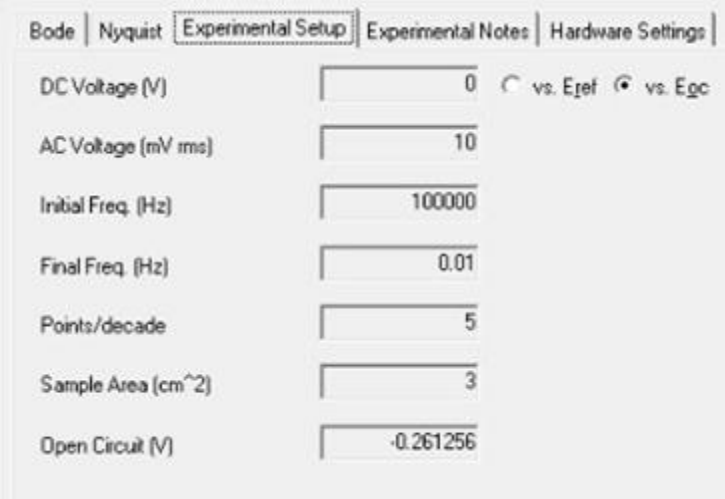

Figure 3 – Test parameters used for the Electrochemical Impedance Spectroscopy experiment used in the GAMRY Software.

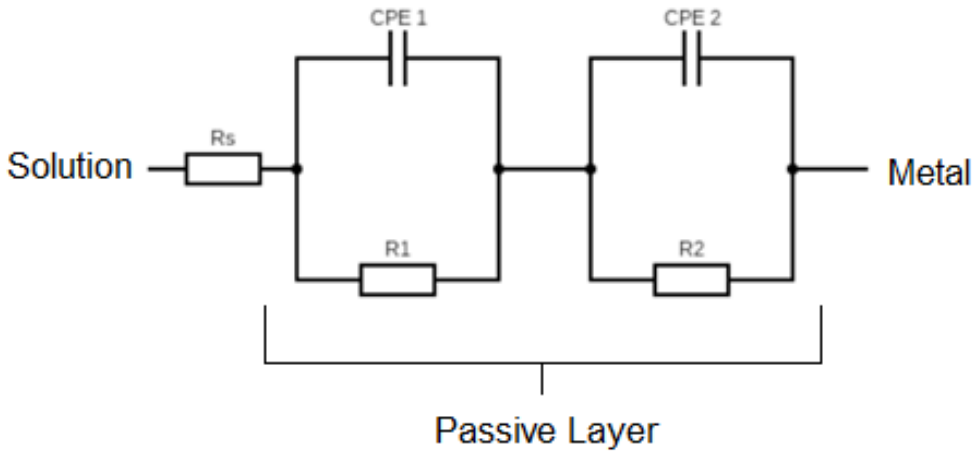

Figure 4 – Equivalent circuit model for the EIS testing where Rs is the solution resistance, CPE is the constant phase element, and R is a resistor. This model represents solution resistance, the passive layer interacting with the solution resistance, and the passive layer interacting with the metal.

(2) Fractography

Optical Microscope Analysis

At the conclusion of the slow strain rate testing, our stainless steel sample will have been completely fractured. It is at this point that we will analyze the fracture mechanics of the material and its level of ductility or brittleness. Different kinds of crack growth will produce different characteristics on the surface. The optical light microscope will be used to take macroscopic imaging and give a high level view of the crack zone. Features that are common during metal failure are radial marks or chevron patterns [28]. As shown in **Figure 5** below, radial marks are lines on a fracture surface that radiate outwards from the origin.

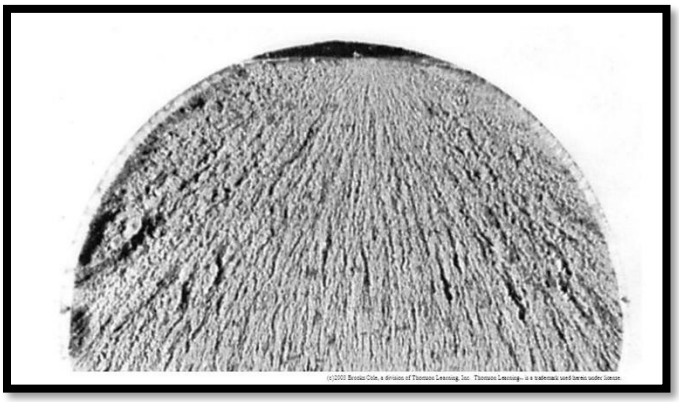

Figure 5 – Chevron pattern in a 0.5 in-diameter 4340 steel after failure.
(© Brooks Cole of Thomas Learning)

An important site that we will be evaluating is the cusp of the failure. This is the point where the rebar was separated into two pieces and is the location of interest. An optical light microscope was used to take images of the sample in different orientations.

Scanning Electron Microscopy (SEM)

A scanning electron microscope produces images of a sample by scanning the surface with a focused beam of electrons to create an image. Electron microscopes are used instead of light microscopes due to electrons having a much shorter wavelength than light, therefore enabling better resolution and higher magnification. Because of this higher level of resolution, SEM machines are extremely valuable during fractography. In ductile failure, the separation of the material at the fracture displays a surface appearance created by microvoid coalescence. These dimples along with many other features are clear indicators of the failure mechanism, such as intergranular fracture or transgranular fracture [28,29].

(3) **Metallography**

The objective of this step is to study the microstructure our samples. The sample will be polished and then electrochemically etched to highlight the grain boundaries of the metal. To begin, our sample will need to be prepared to be mounted. This will entail using rotary cutting disks to remove approximately 2 inch sections from each rebar sample. Samples can be mounted by using either hot thermosetting powder, or cold castable mounting material, commonly an epoxy/hardener combination. Once mounted, the samples will be polished using silica carbide abrasive sandpaper in the following order: 180 grit, 320 grit, 400 grit, 600 grit, 800 grit, and 1200 grit. These samples will be polished for a total of 1-minute intervals at a medium to high rpm (250-300 rpm.) The next step will be replacing the sand paper with a polishing cloth and 9 μm polycrystalline diamond suspension at a low rpm (100-120 rpm.) At the end of polishing, the sample should be rinsed with deionized water before a final rinsing with ethanol/acetone and air hose drying.

In order to highlight the grain boundaries of our sample, an electrochemical etch was performed. This process involved the application of a 6V power source to our sample while in suspension of an 10% oxalic acid solution for approximately 10-20 seconds.

Once the samples are fully prepared, the final step involves using an optical microscope to capture the microstructure. The images taken in this report are at varying magnifications, from 5x magnification to 100x in order to progressively show the analysis location. A basic laboratory set up for the electrochemical etching can be found in the appendix of this report.

(3) <u>Cyclic Potentiodynamic Polarization</u>

Potentiodynamic polarization is a technique used to monitor the corrosion mechanism, rate of corrosion, and susceptibility to corrosion in specific environments. Specifically when dealing with stainless steels, CPP is beneficial for studying the breakdown of the passive oxide film and eventual repassivation. This method involves the combination of both anodic and cathodic polarization to a sample. Meaning that the working electrode becomes more electro-positive during anodic polarization and less more negative during cathodic polarization. These potentials are applied at a continuous, often slow, rate over a range of values, referred to as scan rate and sweep range respectively [25]. In this experiment, a double loop testing technique was used where first the sample stabilizes at its OCP value before being scanned positively

As mentioned above, these potentiodynamic tests are used to extract corrosion rate values. For reactions which are charge or mass transfer controlled, the current density can be expressed as a function of overpotential (η), $E_{app} - E_{ocp}$, known as the Tafel Equation shown in Equation 2 below [26].

$$\eta = \beta \log\left(\frac{i}{i_o}\right) \qquad (2)$$

Where β is the Tafel slope, I the applied current density, and i_o the exchange current density. These slopes can be obtained from the linear regions of the polarization curve as shown in **Figure 6** below. Other important values from these curves include the corrosion potential as well as the corrosion current density. **Figure 7** is in reference to test parameters used for CPP tests.

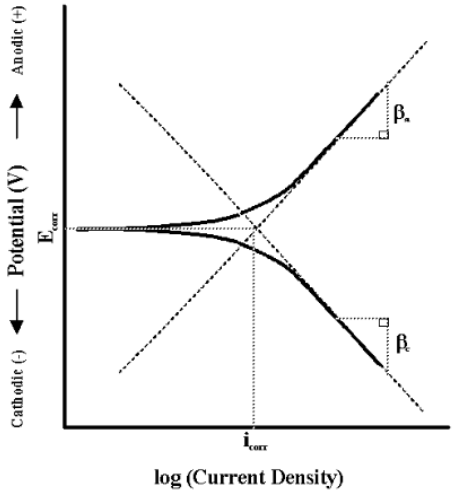

Figure 6 – Example potentiodynamic polarization graph showing cathodic and anodic Tafel slope values, (βa, βc respectively) as well as corrosion current density and corrosion potential.

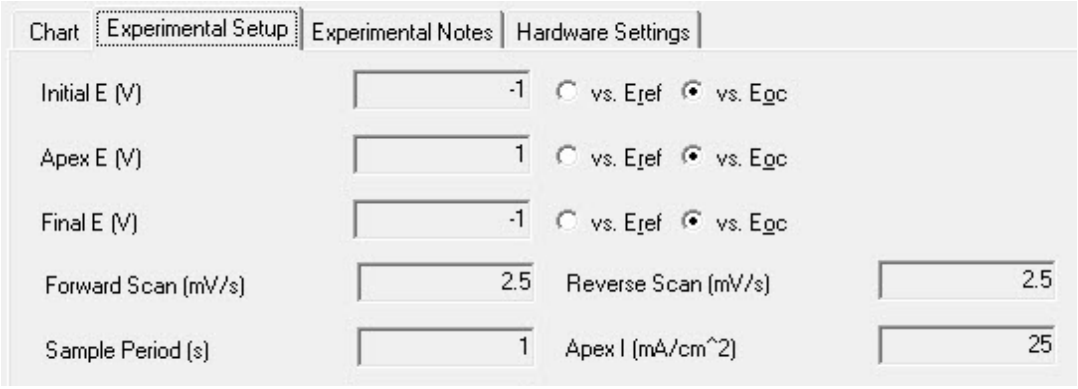

Figure 7 – Test parameters used for the Cyclic Potentiodynamic Polarization experiment used in the GAMRY Software.

3. Results and Discussion

Metallography

Stainless steel AISI 316 has a uniform austenitic structure, meaning all grains will follow a face centered cubic (FCC) crystal structure. This is shown in the metallography images taken, with only a single phase being shown. The etchant used in this circumstance highlights the grain boundaries while also showing carbide inclusions in the grains. This step confirms the phase structure of the sample in question and allows us to proceed as planned.

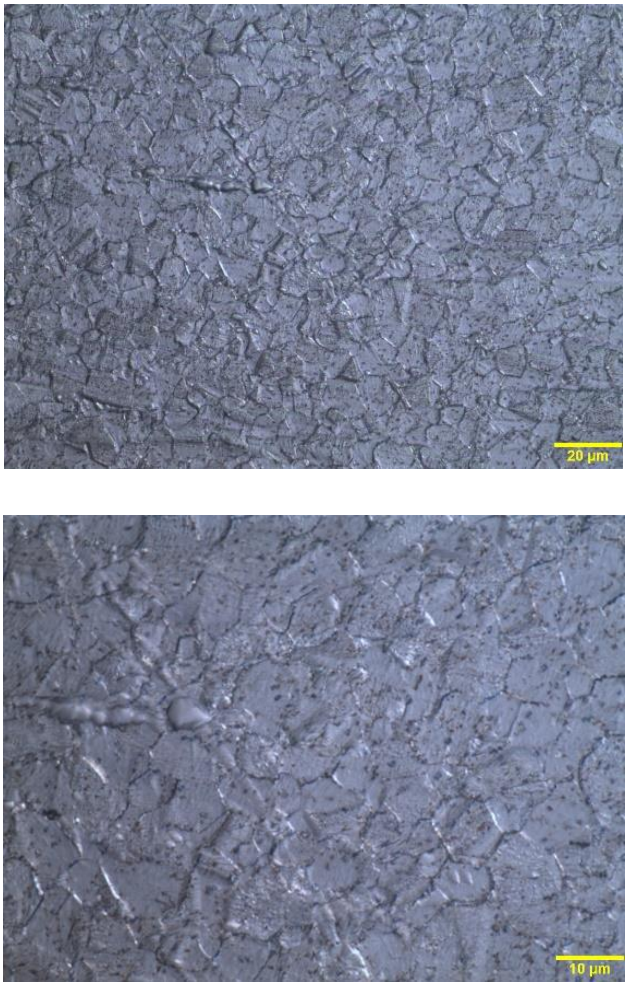

Figure 8 – Metallography images of stainless steel AISI 316 showing a single austenitic phase structure.

Slow Strain Rate Testing

Due to the non-uniform cross sectional area of our sample, a force vs. displacement curve will be used to describe each samples mechanical properties. As shown in **Figure 9** below, the blank sample outperformed the 8% Cl^- sample, reaching an ultimate tensile strength value of 1815 kgf. As expected, due to the presence of the Cl^- ions, the 8% sample performed approximately ~7.7% lesser than that of the blank, only reaching a UTS value of 1675 kgf before beginning to fail.

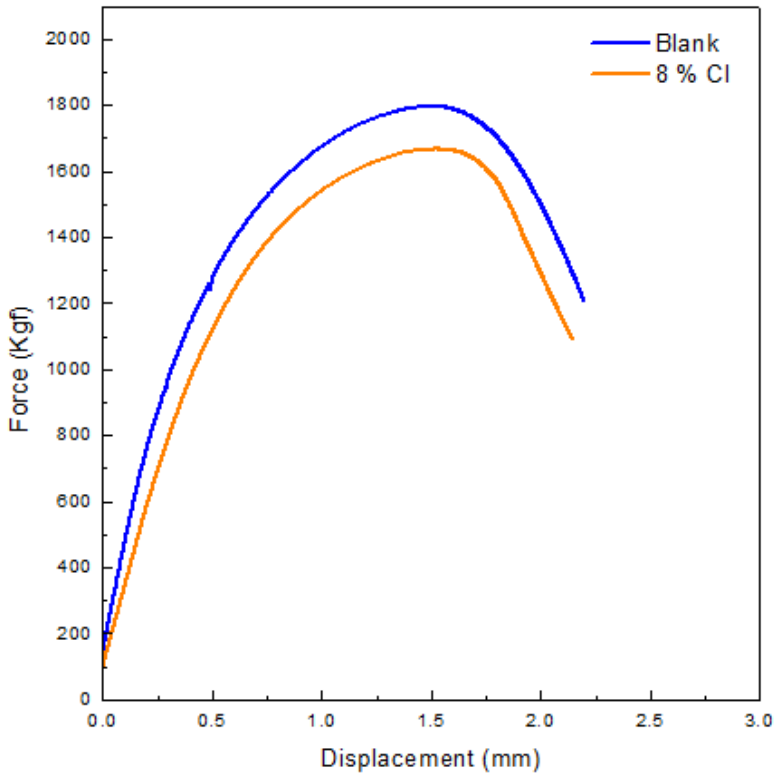

Figure 9 – Force in units of Kilogram-force (kgf) versus displacement (mm) for stainless steel AISI 316 sample. Showing both an 8% Cl^- trial as well as a blank trial.

For the electrochemical tests, the time periods are all relative to this force vs. displacement curves. Once the test was completed, the electrochemical data was fit to parameters within the pre-load range, yield strength range, ultimate tensile strength range, and post failure range. **Figure 10** helps describe how this breakdown was conducted

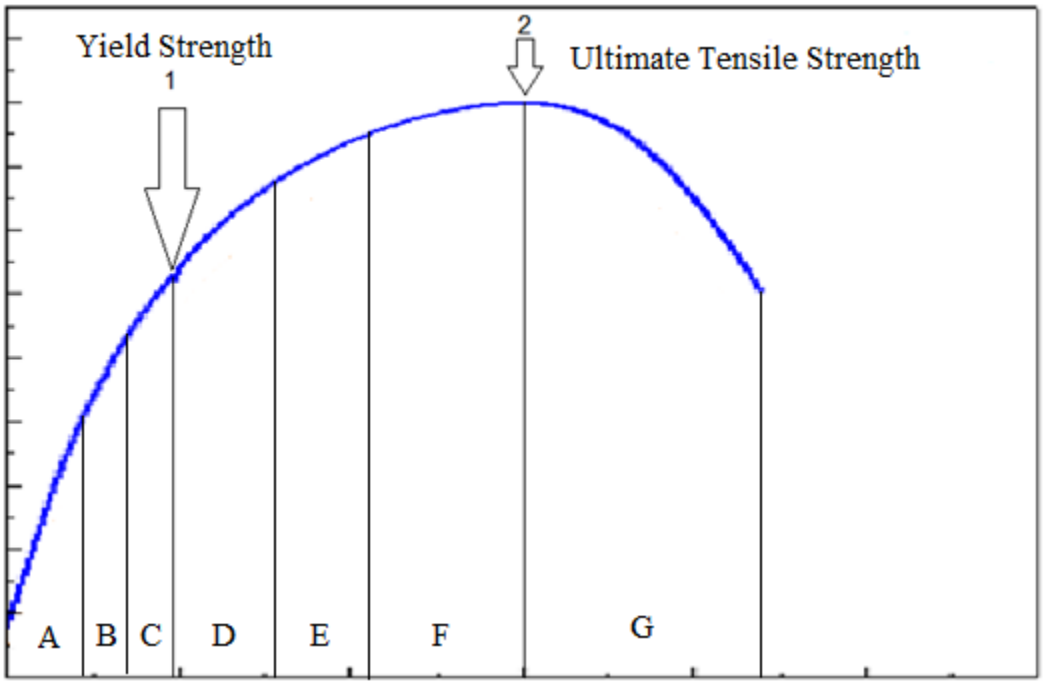

Figure 10 – Sample graph showing how electrochemical tests were conducted based off of force vs. displacement curves. Where point 1 and point 2 on this graph represent the yield strength and the ultimate tensile strength (UTS) respectively. The letters represent the ranges that the tests were conducted over. For example, an electrochemical test labeled 90% UTS would represent the area within letter E.

Linear Polarization Resistance (LPR)

As mentioned previously, the area of interest in a linear polarization test lies in the small linear region produced by the ± 15mV polarization range. This area was analyzed using the GAMRY software to produce Rp values which were then correlated into corrosion rate data presented as mpy, or mils per year. These values, along with E_{corr} and I_{corr} values can be found in **Table 1** below along with **Figure 12** to help describe the trend.

Table 1 – Linear Polarization Resistance data for 8% Cl Stainless Steel AISI 316 Sample. Showing Polarization Resistance (R_p), Corrosion Current (I_{corr}), Corrosion Potential (E_{corr}), and Corrosion Rate in mpy (mils per year)

	R_p (k-ohms)	I_{corr} (µA)	E_{corr} (mV)	Corrosion Rate (mpy)
Preload	34.94	0.745	- 215.2	0.114
50 yield	8.331	3.127	- 312.4	0.476
75 yield	3.061	8.510	- 275.3	1.296
100 yield	5.685	4.583	- 279.7	0.698
80 UTS	2.615	9.964	- 272.0	1.518
90 UTS	4.062	6.414	- 269.2	0.976
100 UTS	2.613	9.970	- 269.9	1.519
Post UTS	1.156	22.540	- 279.2	3.434

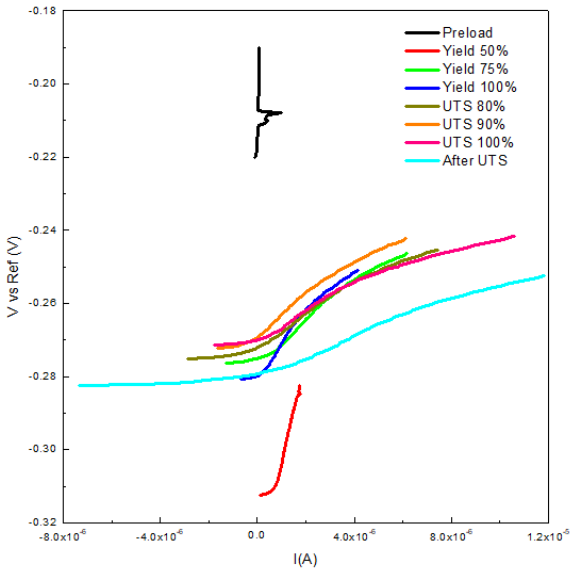

Figure 12 – Linear Polarization Resistance graph for 8% Cl^-, stainless steel AISI 316 Sample. Showing the trend in data across all stages of the sample during tensile testing.

Now analyzing the LPR data, there is an interesting pattern when looking at both the polarization resistance as well as the corrosion rate. It should be noted that for the fitting and use of Equation 1, Tafel slope values of 120 mV were used to calculate corrosion rate values. These values were determined by using the symmetry factor, which is usually 0.5, corresponding to a Tafel slope of 120 mV. At 75% of the yield strength, the corrosion rate spikes to nearly 1.3 mpy. Shortly after, at 100% yield strength, the corrosion rate drops by nearly half to 0.698 mpy, only to rise again to 1.5 mpy at 80% UTS strength. This back and forth phenomena is thought to be the breakdown of the passive oxide film leading to accelerated corrosion rates, before being repassivated and again acting as a corrosion mitigating barrier. Thus highlighting the corrosion resistant properties that stainless steel has when the passive film can be allowed to exist.

Electrochemical Impendence Spectroscopy (EIS)

For the EIS testing, we can compare the results of the 8% Cl^- to the blank to show the differences of the solution on the impedance values. First looking the blank sample (left) in **Figure 13**, we see a very consistent linear relationship across all test fields. This shows minimal activity between the solution and the sample when no Cl^- ions are present to breakdown the passive film. Similar effects that were seen in the LPR test are also seen in the 8% Cl^- sample during EIS testing as well. Whereas impedance values decrease for the 75% yield strength test before then increasing for the 100% yield strength test. Affirming the breakdown and repassivation of the stainless steel passive oxide film and its effects when AC current is applied to the sample

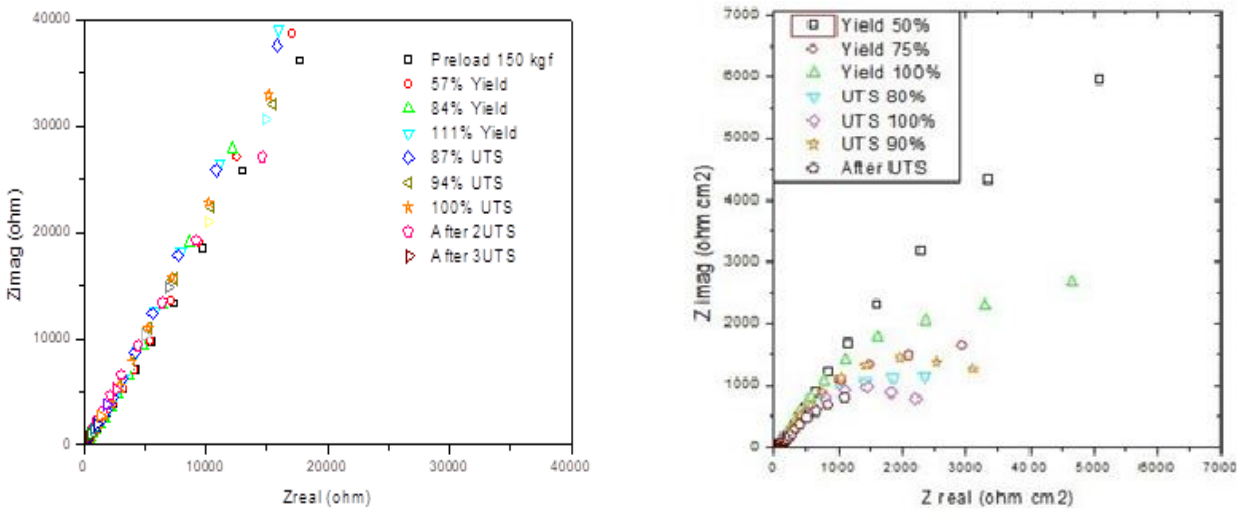

Figure 13 – Electrical Impedance Spectroscopy graphs for blank sample (left) and 8% Cl^- sample (right) for stainless steel AISI 316. Showing the differences between solution resistance Cl^- concentration and its effects on EIS testing.

Cyclic Potentiodynamic Polarization

For this double scan cyclic potentiodynamic polarization test, there is a clear difference between the patterns of each sample. When examining the 8% Cl^- curve, there is a notable repassivation step that is not seen in the blank. Being a destructive testing method, this again hints at the idea of repassivation of the sample. Notable results from this test include the increased corrosion current from blank to the 8% Cl^- sample. The anodic and cathodic Tafel slopes were calculated using the GAMRY software by analyzing the slope of the linear region of the curves near the corrosion current and corrosion potential values.

Table 2 – Cyclic Potentiodynamic Polarization data for both the 8% Cl^- stainless steel AISI 316 Sample as well as the blank. Showing Corrosion Current (I_{corr}), Corrosion Potential (E_{corr}), and the anodic/cathodic Tafel slopes (βa and βc respectively)

Blank, CPP			**8% Cl^-, CPP**	
I_{corr} (A)	7.32×10^{-7}		**I_{corr} (A)**	1.68×10^{-6}
E_{corr} (V)	-4.22×10^{-1}		**E_{corr} (V)**	-3.84×10^{-1}
βa	0.5588		**βa**	0.5524
βc	0.3967		**βc**	0.3513

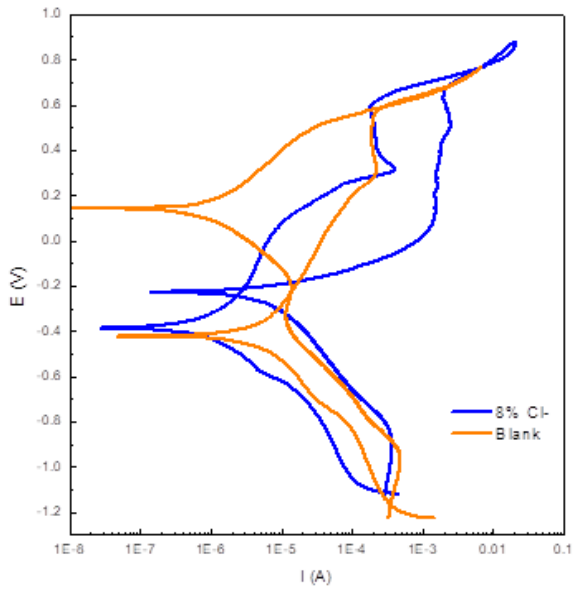

Figure 14 – Cyclic Potentiodynamic Polarization results for both the 8% Cl^- sample as well as blank sample for stainless steel AISI 316. Showing the higher corrosion current when in the 8% Cl^- solution.

Fractography

Beginning with the optical light microscope analysis, images were taken of both the upper and lower parts of the sample. Reflecting which end was in the upper arm of the tensile machine and which end of the rebar was in the static lower arm. Examining the blank sample **Figure 15**, we can see a clean fracture with very little corrosion product buildup. There is a slight cusp on the bottom sample which has been highlighted. Now when examining the 8% sample, there are signs of corrosion product buildup on the upper sample. Whereas this was not seen on the blank, this buildup can be attributed to the presence of chloride.

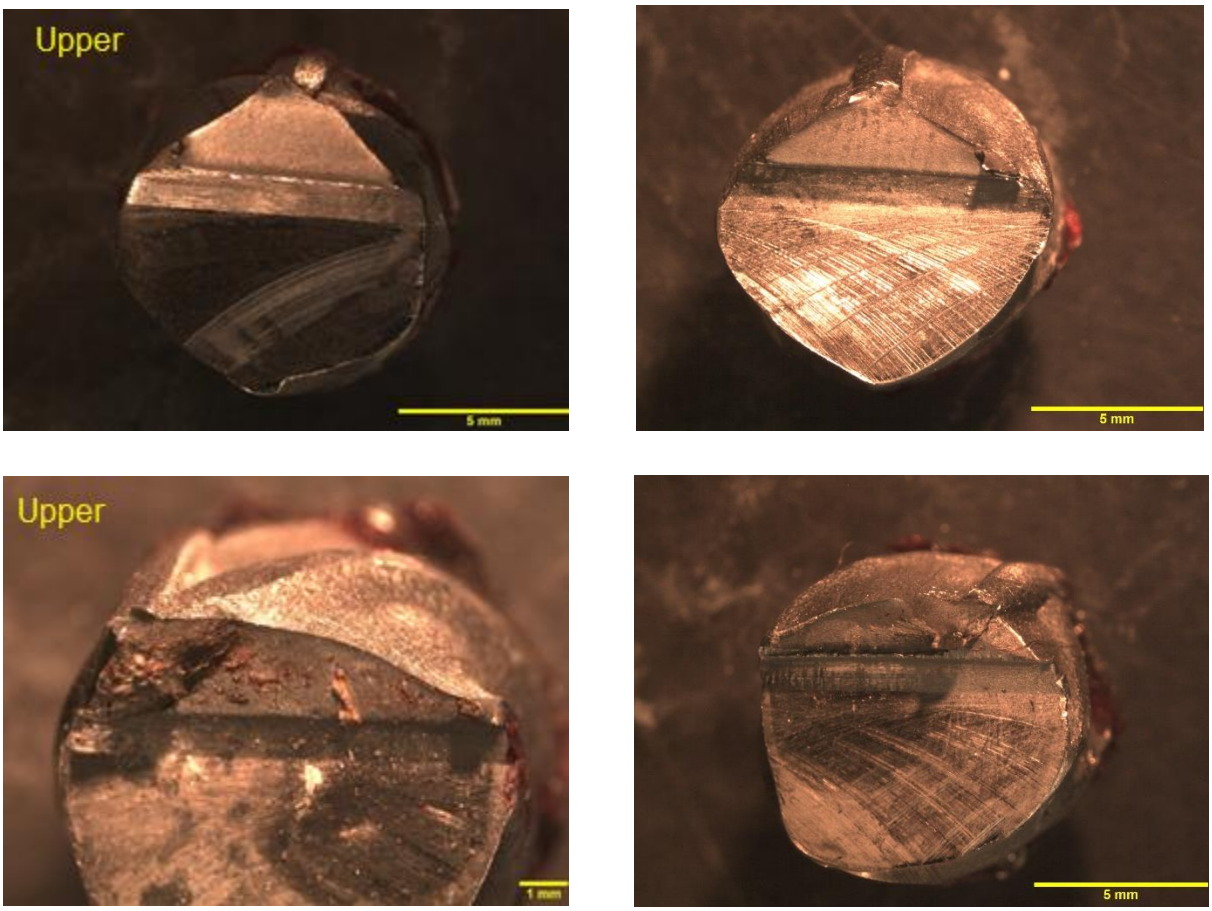

Figure 15 – Optical light microscope images of the stainless steel 316 blank sample (top row) and 8% sample (bottom row)

The Scanning Electron Microscope (SEM) was used for a higher resolution image of the fractures. When examining **Figure 16** below, we see signs of intergranular cracking in the upper left image. Seeing these grain boundaries helps better understand the Stress Corrosion Cracking mechanism for this particular stainless steel. Also in this image we can see what looks like dimples in the material, referring to a collection of micro voids along the grain boundaries of the metal. The occurrence of these micro voids is directly proportional to increased corrosion rate and fracture rate [31].

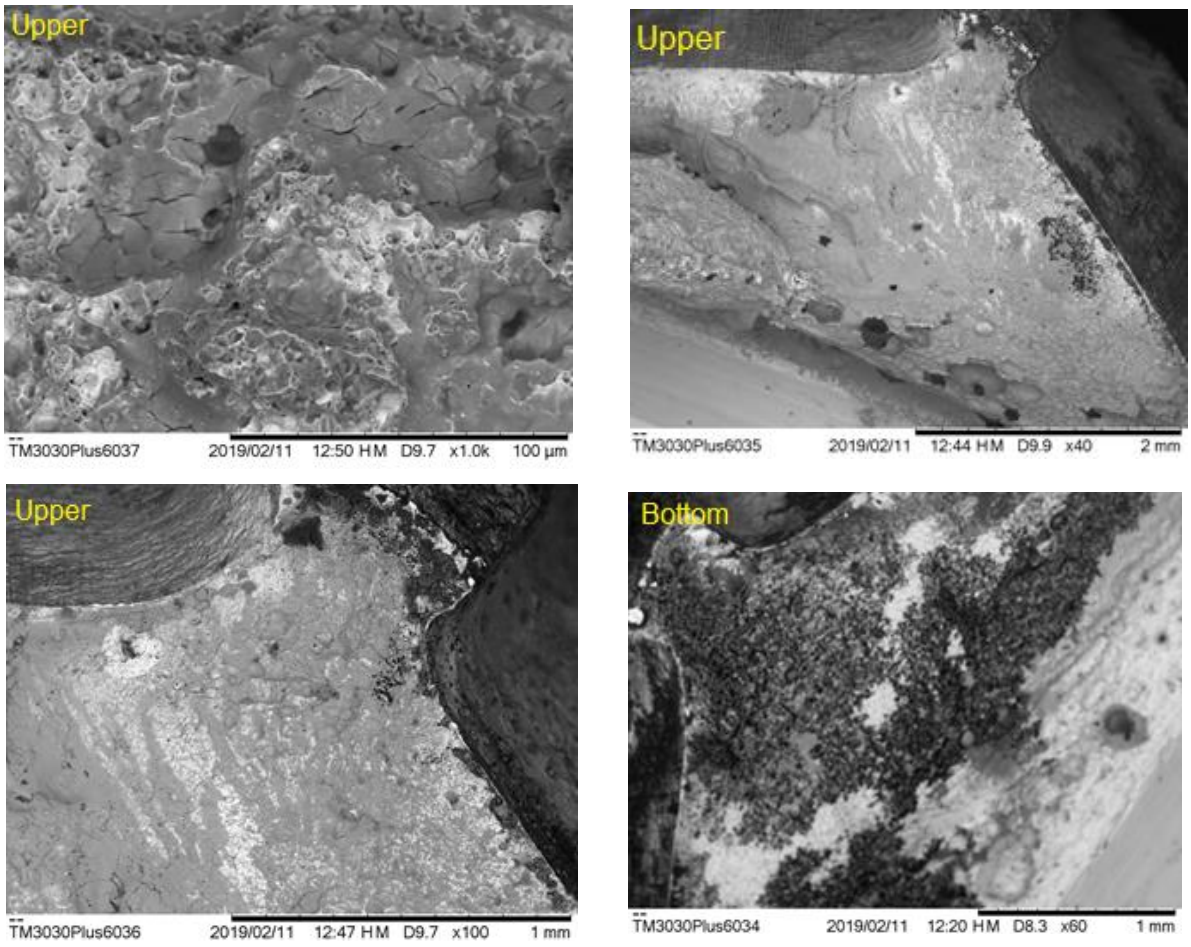

Figure 16 – Scanning Electron Microscope images of stainless steel AISI 316 8% Cl sample with both upper and lower sample ends.

4. Conclusions

With the overall goal of this research to develop a relationship between electrochemical and mechanical properties of stainless steel rebar, this is impossible to conclude based off information in this report. Due to difficulties in testing, we were unfortunately only able to confidently report the values of the blank SS AISI 316 sample and the 8% Cl SS AISI 316 sample. With that being noted however, there are results in these two data sets that support our set out ideologies. Starting with the LPR and EIS tests, there are signs of film breakdown and repassivation in the 8% Cl data set that simply is not visible in the blank sample. This led to higher corrosion rate values during times of passive oxide failure and would therefore lead to a shorter life span of the rebar. This was reflected in both the fractography as well as the tensile test results. When examining the optical light microscope fractographic images, we see very clear signs of corrosion product buildup on the upper arm of the 8% Cl sample. It is believed that this buildup could actually lead to accelerated corrosion by assisting in the separation of the sample. The electrochemical data is then supported by the mechanical results from the stress/strain curve after tensile testing. The 8% Cl^- sample yielded an ultimate tensile strength approximately 7.7% less than that of the blank sample (140kgf).

Although no absolute conclusions can be made from the current data gathered, there are signs that point in the right direction for this research. Lesser mechanical properties and higher corrosion rate data based off of passive film breakdown by Cl^- ions is what was expected and also what was gathered. The importance of this topic and the value it can bring to the industry in terms of both safety and accurate life cycle costing mean that research must continue. Over the following months, Ulises and Dr. Bastidas will continue to test the remaining four samples in order to reach our goal.

5. Acknowledgements

This research paper is a cumulative reflection of my five years here at the University of Akron. Enrolling in the brand new corrosion engineering program was the best decision of my life and it has been a privilege to see the curriculum and staff grow. I would like to thank all of my professors for helping me achieve the level of success that I have reached at this point in life. I will be entering the work force right out of college as a full time project engineer with Marathon Petroleum Corporation. A level of success I dreamed about as a freshman joining this program is now coming into fruition.

In regard to this Honors Project, I would like to thank Dr. Bastidas for allowing me to assist him in his research and use his laboratory facilities. With going into a full time engineering role this May, it was extremely valuable to know the research side of the industry and what lab testing entails. The topic of stress corrosion cracking is also pertinent in the pipeline world and information gained here will translate to my work as well. I would also like to thank Ulises Martin Diaz for assisting me in the day-to-day work in the lab. It was an enjoyable experience to work through challenges with each other and I feel like we both benefitted from the time spent together.

6. Literature Cited

[1] Barton Rebar Steel Supply. “How Stainless Steel Rebar Is Used in Reinforced Concrete Construction.” *Barton Supply Co.*, 13 June 2017, barton-supply.com/2017/06/14/how-stainless-steel-rebar-is-used-in-reinforced-concrete-construction/

[2] Popov, Brandon N. Corrosion Engineering: Principles and Solved Problems. “*Chapter 9: Stress Corrosion Cracking”*. 26 June 2015.

[3] ISO 7539-11 (2013). Corrosion of metals and alloys – Stress corrosion testing

[4] “Modelling Corrosion Propagation in Reinforced Concrete Structures – A Critical Review.” NeuroImage, Academic Press, 17 Nov. 2010

[5] British Stainless Steel Association. “BRITISH STAINLESS STEEL ASSOCIATION. Making the Most of Stainless Steel.” *How Many Types of Stainless Steel Are There?*, 2017, www.bssa.org.uk/faq.php?id=10.

[6] American Welding Society. “Classifications of Stainless Steel Rebar.” *Classifications of Stainless Steel* , 2017, app.aws.org/wj/1998/11/kotecki/.

[7] Berglund, Peter L. “Austenite.” *Austenite*, 2006, threeplanes.net/austenite.html.

[8] Nickel Institute. “Stainless Steel: The Role of Nickel.” *Stainless Steel: The Role of Nickel | Nickel Institute*, 2014, www.nickelinstitute.org/about-nickel/stainless-steel/.

[9] Saefong, Myra. “Why Nickel Prices Have Skyrocketed This Year.” *Marketwatch*, 15 May 2014, blogs.marketwatch.com/thetell/2014/05/15/why-nickel-prices-have-skyrocketed-this-year/.

[10] “Base Metal Stocks and Price Charts.” *Base Metals Stocks and Price Charts | KITCO Metals*, 2019, www.kitcometals.com/charts/.

[11] BNProducts. “What Are the Different Types of Rebar? And Does It Matter?” *BN Products*, 25 Oct. 2018, www.bnproducts.com/blog/what-are-the-different-types-of-rebar-and-why-do-types-matter/.

[12] “Duplex Stainless Steel, Lean Duplex and Super Duplex.” *Montanstahl*, 10 Apr. 2018, www.montanstahl.com/blog/duplex-stainless-steel-lean-duplex-super-duplex/.

[13] “Seawater.” *Seawater*, 2019, www.cs.mcgill.ca/~rwest/wikispeedia/wpcd/wp/s/Seawater.htm.

[14] “Introduction to Tensile Testing”, *ASM International Chapter 1”* 2004. Asminternational.com

[15] Harris Supply International. “Harris Supply Solutions.” *Harris Supply Solutions*, www.harrissupplysolutions.com/rebar-guide.html.

[16] Satyendra. “Steel Reinforcement Bars and Its Important Characteristics.” *Ispatguru.com*, July 2014, ispatguru.com/steel-reinforcement-bars-and-its-important-characteristics/.

[17] Instron. “Tensile Testing.” *Instron*, 2013, www.instron.us/en-us/our-company/library/test-types/tensile-test.

[18] Jones, R.H. Ricker, R.E. “Mechanisms of Stress-Corrosion Cracking” Chapter 1. 1992. *Pacific Northwest Laboratories, National Institute of Standards and Technology*

[19] Marchand, David. “Fractography.” *Nanoscience Instruments*, www.nanoscience.com/applications/materials-science/fractography/.

[20] “Open Circuit Potential Vs. Time.” *BASi®*, www.basinc.com/manuals/EC_epsilon/Techniques/CPot/ocp.

[21] “Getting Started.” *Polarization Resistance Tutorial*, 2015, www.gamry.com/application-notes/corrosion-coatings/corrosion-techniques-polarization-resistance/.

[22] “Linear Polarization Resistance and Corrosion Rate” *Theory and Background*. 2014 Pine Research

[23] Corrosion Doctors. “Potentiodynamic Polarization.” *Potentiodynamic Polarization*, corrosion-doctors.org/Electrochem/PotPol.htm.

[24] Esmailzadeh, S. “Interpretation of Cyclic Potentiodynamic Polarization Test Results for Study of Corrosion Behavior of Metals: A Review” 2017. “Investigation Methods for Physicochemical Systems

[25] Perumarredi. “Potentiodynamic Polarization.” *Potentiodynamic Polarization - an Overview ScienceDirect Topics*, 2003, www.sciencedirect.com/topics/chemical-engineering/potentiodynamic-polarization.

[26] Enos, David. “The Potentiodynamic Polarization Scan.” *Ameteksi.com*, 1997.

[27] “Application Electrochemical Impedance Spectroscopy Methods to Evaluation Corrosion Behavior of Stainless steels 304 in Nanofluids Media”. 2015. International Conference on Advances in Nuclear Science Engineering.

[28] Parrington, Ronald J. “Fractographic Features in Metals and Plastics”. *ASMInternational*. 2008. www.asminternational.com.

[29] “Scanning Electron Microscopy.” *Nanoscience Instruments*, 2014, www.nanoscience.com/techniques/scanning-electron-microscopy/.

[30] Beaudoin, J.J. “Calcium Hydroxide in cement matrices: physico-mechanical and physico-chemical contributions. 2000. National Research Council

[31] https://www.corrosionpedia.com/definition/6168/dimple-fracture

[32] ASTM-G129, “Standard Practice for Slow Strain Rate Testing to Evaluate the Susceptibility of Metallic Materials to Environmentally Assisted Cracking

[33] Bastidas, D.M., Briz, E.B. “Stress Corrosion Cracking of New 2001 lean-duplex stainless steel reinforcements in chloride contained concrete pore solution: An Electrochemical Study” (2018) Construction and Building Materials 192, pp. 1-8

Appendices

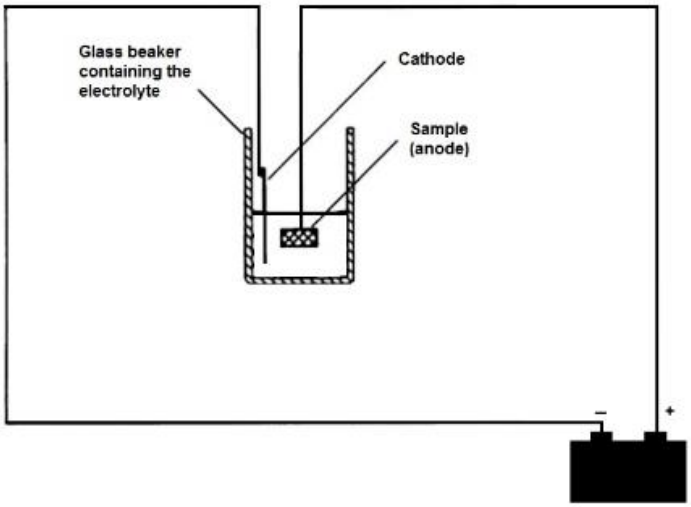

Basic laboratory setup for electrolytic etching

Appendix Image 1 - This was a basic laboratory set up that was used for our electrochemical etching. Using 10% oxalic acid and an applied voltage of 3-4V, the samples were etched in 15-30 seconds.

Appendix Image 2 – Sample image of a threaded rebar, coated in red lacquer with the notch exposed allowing for electrochemical tests to be focused on this region.

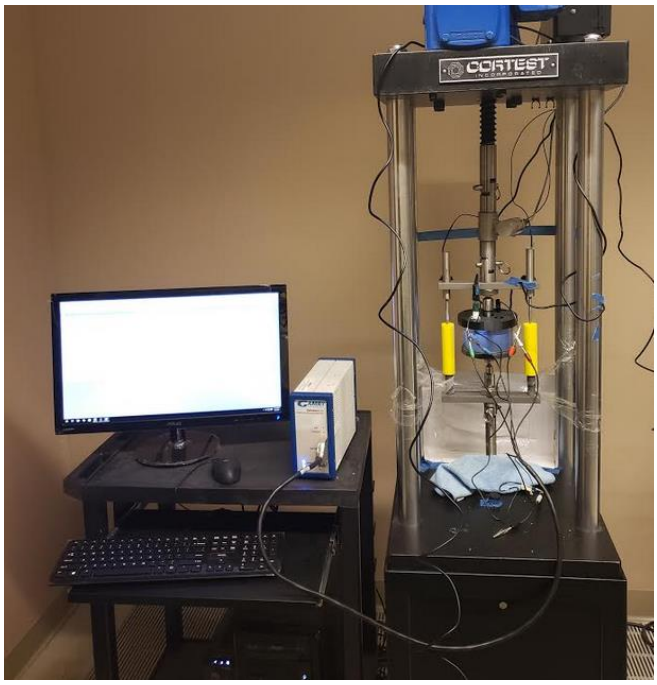

Appendix Image 3 - The overall basic laboratory set up that was used for our tensile testing. Fit with an electrochemical cell and connected GAMRY potentiostat.

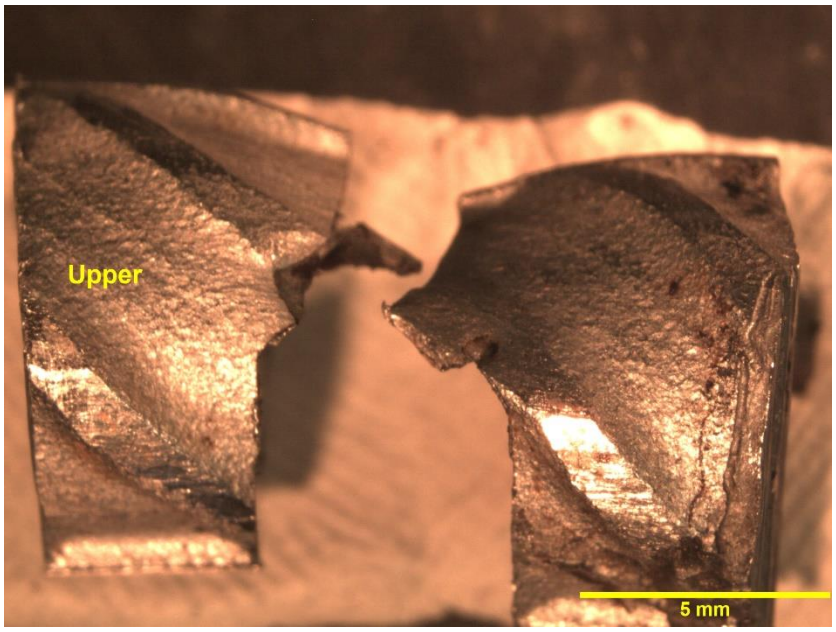

Appendix Image 4 – Additional fractography image using optical light microscope showing the cusp and connection between the upper and bottom fractured rebar.